GRC Transactions, Vol. 41, 2017

Review of Exploitable Supercritical Geothermal Resources to 5 km at Geysers-Clear Lake, Salton Sea, and Coso

Jim Stimac[1], Maxwell Wilmarth[2], Petronila Esther Mandeno[3], Patrick Dobson[4] and Jeff Winick[5]

[1]Stimac Geothermal Consulting, 4210 Chaparral Rd., Santa Rosa, CA 95409

[2]Geologica Geothermal Group Inc., 5 Third St, Suite 420, San Francisco, CA 94103

[3]Digital Mapping Solutions, P.O. Box 7254, Cotati, CA 94931

[4]Energy Geosciences Division, Lawrence Berkeley National Laboratory, Berkeley, CA 94720

[5]BCS, Incorporated, 7828 Vance Drive, Suite 103, Arvada, CO 80003

Keywords

Supercritical geothermal resource assessment, brittle-ductile transition, EGS, The Geysers, Clear Lake, Salton Sea, Coso, GeoVision

ABSTRACT

The U.S. Department of Energy (DOE) has commissioned a preliminary assessment of domestic supercritical geothermal resources as part of a wider evaluation of “blue-sky” technologies in support of the Geothermal Technologies Office’s GeoVision study. Supercritical Geothermal Potential is estimated for The Geysers-Clear Lake, Salton Sea, and Coso areas to a depth of 5 km below ground surface. All three areas show evidence for relatively recent (≤50,000 years) shallow intrusion of magma resulting in supercritical conditions at this depth. We draw upon wide ranging studies and interpretations that constrain the extent of the supercritical domain. Most of these sources are publicly available, but some additional data were provided by field operators.

Introduction

The U.S. Department of Energy's Geothermal Technologies Office (GTO) is engaged in a *GeoVision* study; a multi-year research collaboration amongst national laboratories, visionary experts from industry, and academia aimed at identifying a vision for growth of the U.S. geothermal industry based on R&D advancements in cost reduction and improved performance across the full range of geothermal resources and technologies. The goal of the *GeoVision* study is to explore the potential contribution of geothermal energy to the U.S. economy and to expand the utilization of geothermal resources in order to increase the nation's economic development and energy security through reliable, resilient, and flexible contributions to a diverse energy portfolio.

In support of the wider *GeoVision* effort, DOE is evaluating a range of "blue-sky" technologies which are potential game-changers for the domestic geothermal industry. Electricity generation potential from supercritical geothermal resources has been recognized globally as one of the key "blue-sky" technologies worthy of significant attention (Dobson et al., 2017). It has long been recognized that a massive heat resource exists in the U.S. related to relatively shallow magmatic intrusion (Smith and Shaw, 1975, 1978; Tester et al., 2006). The shallowest and most permeable parts of these intrusive-hydrothermal systems have been exploited by conventional means since the 1960's, but their deeper and less permeable roots have remained largely untapped. These potentially vast unconventional resources have been referred to as Enhanced Geothermal Resources (Tester et al., 2006; Augustine, 2016). The technologies needed to exploit them, and their ultimate potential have been investigated for decades, but commercial exploitation has remained elusive. The U.S. DOE's *GeoVision* study will elaborate a roadmap of actions to be undertaken by a range of stakeholders that will help achieve the outcomes of the *GeoVision* effort, ensuring maximum benefit to the nation. This will include a technical roadmap to initiate development of a suite of next-generation technologies required to cost-effectively develop supercritical resources.

1. Supercritical Systems

In areas of shallow magma intrusion it is expected that rocks reach the brittle-ductile transition (370-400°C) and the critical point of water (374°C and 221 bars) at drillable depths with current technology. However this potential resource has remained largely unexploited due to the challenges and costs of deep, high-temperature drilling, and uncertainty on how to most effectively mine the heat energy contained within what is presumed to be low permeability rocks. This report focuses on assessing the potential supercritical geothermal resource in three areas with very large conventional geothermal systems related to magma intrusion: The Geysers-Clear Lake, Salton Sea, and Coso areas. If EGS exploitation of near-intrusive regions becomes economic, it is likely to be successful first in one of these well-studied areas, and then expanded to other volcanically active regions where commercial activities are not prohibited or unwise due to the eruption hazard.

The approach taken in this study is to assume that the significant technological barriers to harnessing this potential resource can and will be overcome, and that the resource can be exploited economically in the future to a depth of at least 5 km below average ground surface.

Similar resource assessment efforts underway in other countries were recently summarized by Dobson et al. (2017) and references therein.

1.1 Definition of Supercritical Conditions

The critical point for pure water is Tc ~ 373.9°C (705.1°F), Pc ~ 220.5 bars (3197.5 psi), and fluid density of ~ 0.323 g/cm3. Both Tc and Pc are raised by salinity and reduced by dissolved CO2. For example, the critical point for seawater (~3.5% salinity) is 405°C and 302 bars. Salton Sea geothermal fluids have extremely high salinities of 20-30%, and thus have supercritical temperatures of ~550°C (Driesner and Heinrich, 2007). For simplicity we maintain our resource estimation cutoff based on a temperature of 374°C.The low density and viscosity of supercritical fluids results in greatly improved transport properties that are predicted to result in much higher flow rates from wells, even when permeability is low (e.g., Friðleifsson et al., 2007; Elders et al., 2014). These fluids also have high rates of mass transport because of their much higher ratios of buoyancy forces relative to viscous forces in the supercritical state (Elders et al., 2014). In addition, ultra-high enthalpy production translates to higher steam rate, higher wellhead pressure, and better energy conversion than in typical conventional geothermal systems.

The transition to supercritical conditions is approximately coincident with the transition from brittle to ductile rock behavior, and in an environment where magmatically dominated fluids may be present (Fournier, 1991, 1999). The transition from brittle to ductile behavior of common rock materials is expected in the range from 370-400°C and approaching these conditions, quartz develops retrograde solubility, and thus may precipitate from the pore fluids and seal naturally occurring permeability (Fournier, 1999; Neilson et al., 2001; Scholz, 2002, Dobson, 2017). This is consistent with a commonly observed limit of about 320-360°C maximum measured temperatures in commercially productive geothermal wells worldwide. In Iceland, the brittle-ductile boundary at the Reykjanes, Hengill, and Krafla geothermal fields occurs at 4-5 km based on a sharp drop in seismicity below this depth (Friðleifsson et al., 2014). However, at this depth, temperatures are often 600°C or greater; this shift to higher temperatures for the brittle-ductile boundary is presumably due to the rock properties of the basaltic crust. The brittle-ductile transition in the Northwest Geysers also appears to be deeper than the transition to supercritical conditions, as numerous microseismic events occur 1.0 to 1.5 kilometers below the static, conductive rock temperature of 400°C measured at 3.4 km depth.

1.2 Definition of Drillable Depths

Supercritical conditions exist everywhere in the Earth deeper than perhaps 30-50 km, however these depths are inaccessible by current or near-term drilling technology. The deepest scientific borehole ever drilled is in Russia with a depth of 12,262 m (Osadchy, 2017). The deepest commercial boreholes are oil wells such Oklahoma's Bertha Roger's well (9,583 m) (American Oil and Gas Historical Society, 2017) and the deepwater Tiber well (10,685 m) off the coast of Texas. Oil and gas wells are routinely drilled to depths of ~5 km. Geothermal wells are typically only economic to 3.5 to 4 km, with some wells drilled to ~4.5 to 5 km in Bavaria (Knapek and Platl, 2014).

This study assesses supercritical geothermal resources to a depth of 5 km below ground surface because this is attainable and is no more than about 1 km beyond the typical maximum depth of economic geothermal wells. We emphasize that the supercritical resources evaluated in this study grow significantly larger below this depth, but this extension cannot currently be accessed economically with existing drilling technology.

1.3 Definition of Brittle-Ductile Transition Zone

The brittle-ductile transition in rocks is only qualitatively understood. Scholz (2002) prefers using "brittle-plastic transition" to "brittle-ductile" and defines it as where deformation occurs as easily by dislocation as by crack propagation. Brittle deformation results in a volume increase that is favored at low confining pressure. Dislocation glide requires no volume change and is therefore insensitive to pressure and favored by increasing depth of burial and temperature. This transition is gradual, depending on many factors including rock and mineral composition and strain rate.

The transition to ductile conditions occurs at the level in the crust where the downwards increasing brittle strength equals the upwards increasing ductile strength. This zone is, therefore, the strongest part of the crust and the depth at which many earthquakes occur. At more plastic conditions, earthquakes are fewer, making the transition approximately equivalent to the base of the seismogenic zone. The depth to ductile rock is shallower for slow deformation and/or for high heat flow and deeper for fast deformation and/or low heat flow.

1.4 Permeability in the Near-Intrusive Environment

Heat transfer in ductile rocks is expected to be dominantly by conduction due to very low permeability caused by the plastic nature of the rock mass and the retrograde solubility of quartz, which might rapidly seal new fractures (Fournier, 1991; Tsuchiya and Hirano, 2007; Saishu et al., 2014). However, laboratory experiments on fractured granite suggest that there is not a necessarily a step-function decrease in permeability associated with the brittle-ductile transition, and that potentially exploitable resources may occur in nominally ductile granitic rock at temperatures of 375-460°C and depths of 2-6 km (Watanabe et al., 2017).

In this study we are interested in constraining the range of permeability in the near-intrusive region where temperatures are above the critical point for pure water. It is known from numerous deep geothermal wells that the permeability of this domain is very low (e.g., Dobson et al., 2017 and references therein). Most of the rock mass is probably at or below the threshold permeability of convection, <0.001 millidarcy (1 microdarcy or $1x10^{-18}$ m^2). However, some active fault and fracture systems may be present that have the permeability required for convective geothermal upflow plumes, estimated by Rowland and Simmons (2012) at $1x10^{-16}$ m^2 (or 0.1 md). Norton and Hulen (2001) cited evidence for permeability of 0.01 to 1 millidarcy ($1x10^{-17}$ m^2 to $1x10^{-15}$ m^2) in various near-intrusive environments. Bulk permeabilities of 0.1 to 1 millidarcy are probably required to deliver commercial fluid production rates, even with the anticipated enhanced flow properties and high enthalpies of the supercritical domain. Thus finding or stimulating permeability in this range or above is one of the greatest challenges inherent in supercritical geothermal exploitation.

2. The Modeling Approach Used in this Study

In this study 3D interpolations of temperature were constructed using Leapfrog Geothermal Software©, using a variety of hard and soft input data described below. Temperature shells were mapped to a depth of about 5 km below the average surface elevation in each area. Each shell was evaluated separately in 3D and their areas summed to estimate the total extent of temperatures exceeding the critical point (assumed as 374°C). Table 1 summarizes model boundaries, units, and cutoff elevations for each resource modeled.

Table 1. Model coordinate systems, boundaries, units, average surface elevation, and elevation of base cutoff.

		Model Units			Bounding Coordinates							
Field	Projection	Coordinate System	Elevation	Temperature	West (left)	North (top)	East (right)	South (bottom)	Model Resolution	Average Elevation of Model Area (rsl)	Average Elevation Used (m rsl)	Base Cutoff Elevation (m rsl)
Coso	UTM, Zone 11, NAD83/WGS84	meters	meters	deg C	414950	4000800	445950	3973300	100 m	1541 m	1100*	-3900
Geysers-Clear Lake	UTM, Zone 10, NAD83/WGS84	meters	meters	deg C	496940	4328410	556580	4272530	500 m	406 m	406 m	-4594
Salton Sea	California State Plane, Zone VI, NAD83	feet	feet	deg F	6714760	2047140	6799240	1970630	500 feet	-172 feet	-52	-5052

*Coso elevation was adjusted to 1100 m since it was more typical of the actual anomaly area than the regional average.

The main hard data used in this study were measured temperatures, especially in deep wells (≥2000 m). Shallower wells were also used to define the extent of regions of anomalous heat flow, and establish boundary conditions. Wells with deep conductive gradients were used to linearly extrapolate those trends to greater depths beyond bottom hole. In most cases R^2 values were better than 0.96, but in a few cases fits as poor as 0.90 were accepted and extrapolated. Poorer fits were only utilized if no other data were available.

"Bottom-up" inferences about temperature were also employed. Where available, thermal modeling studies that matched shallow temperature or heat flow trends through simulation of magma emplacement (typically 4 km or deeper) were also considered (e.g. Clear Lake-Geysers, Salton Sea). These studies were used to infer temperatures below drilled depths or where no well control was available.

Soft data included a wide variety of geologic, geophysical and geochemical information that provided insight to the distribution of major structures, the timing of volcanism and associated intrusion, and indications of ductile conditions. In particular the depth to the base of the seismogenic zone was used. Other geophysical methods such as gravity, magnetics, and resistivity were only used as general indicators of the likelihood of intrusion depth and extent.

Once the volume of rock at supercritical conditions was estimated, the amount of contained heat was calculated using the midpoint temperature of each shell, and a range of "recovery factors" applied to estimate the supercritical geothermal resource base. We were mindful that application of this method has grossly overestimated resource potential in some studies (see Grant, 2015), and we therefore applied conservative recovery factors as described later. It is possible that revolutionary technological advancement could achieve greater recovery of heat than has been estimated here.

3. The Geysers/Clear Lake Area

The Geysers-Clear Lake area represents one of the largest areas of anomalous heat flow in the US (Walters and Combs, 1991; Stimac et al., 1997) and The Geysers is still the largest conventional geothermal producer in the world after 57 years of production (Sanyal and Enedy, 2011). More than 600 wells have defined an area of convective circulation of at least 105 km^2. The peak power capacity of the field exceeded 2000 MW, but was not sustainable, and the current field production levels are on the order of 850 MWe. In the adjacent and related Clear Lake area, volcanism as young as 0.09 Ma (Borax Lake centers) has been identified (Donnelly-Nolan et al., 1981).

Since most of the silicic volcanism at Clear Lake is older than 0.3 Ma, it is likely that shallow intrusions are in an advanced state of solidification and that cooling granitic bodies might be located at drillable depths. This is significant because future EGS or supercritical geothermal systems may be hosted within or at the roof of these systems, analogous to The Geysers.

3.1 High and Normal Temperature Reservoir

Early drilling in the NW Geysers identified High Temperature Reservoir (HTR). In this part of the reservoir, the normal steam-dominated zone is underlain by a region of steep conductive temperature gradients (Walters et al., 1992; Walters and Beall, 2002; Beall and Wright, 2010). Temperatures above 350°C have been measured in many wells (Walters et al., 1992; Stark, 2003; Garcia et al., 2012, 2016). The highest temperatures were encountered in well Prati-32 at 3352 m with a measured temperature of 400°C. The top of the HTR forms a broad dome at elevations of 1.8 to 2.4 km bsl (Stark, 2003; Beall and Wright, 2010). Where the HTR is permeable, it also produces dry steam with higher non-condensible gas (NCG) than the normal temperature reservoir NTR. Volatile chloride in superheated steam causes corrosion when it condenses, making production from this area more problematic.

3.2 Measured and Interpolated Thermal Gradients

Walters and Combs (1991) compiled temperature and thermal conductivity data from a large number of shallow gradient wells throughout the Clear Lake-Geysers area. They defined regions of anomalous heat flow that included the entire region of The Geysers reservoir and the main silicic volcanic centers of Clear Lake.

Two and three-dimensional thermal modeling by Erkan et al. (2005) suggested that the observed heat flow required an extensive region of long-term (1 Ma) low-rate 0.005 km^3/yr) magma emplacement at <10 km depth under the entire area of the Geysers-Clear Lake thermal anomaly. Their 3D inverse models of intrusion predict supercritical temperatures beneath much of The Geysers at 4 km, and over much of the area of silicic volcanism at 6 km depth. Their inferred deep temperatures were utilized in our model.

3.3 Seismic Constraints on Upper Crustal Magma and Brittle-Ductile Transition

There is no clear geophysical evidence for active magma bodies beneath The Geysers reservoir, although heat flow data described above suggest relatively recent emplacement of magma in the NW Geysers. There is some evidence for relatively recent shallow magma emplacement in the Clear Lake area.

There is a long history of studies detecting teleseismic velocity lows in the Clear Lake area consistent with the modern paradigm of magma bodies with small melt fraction or magma mush columns, rather than large reservoirs of pure liquid. It is also consistent with a long history of small batch magma emplacement over the area (Stimac et al., 1997; Erkan et al., 2005).

It has been observed that there is a good correlation between the location and timing of microearthquakes (MEQs) and water injection at The Geysers (Stark, 1990; 2003; Majer and Peterson, 2007; Hartline et al., 2015). It has even been inferred from steam chemistry and production data that the distribution of MEQs approximately images the distribution of injected liquid (Stark, 1990). It has also been observed that some MEQ clusters reach kilometers below the bottoms of injection wells.

3.4 3D Temperature Model

An average ground elevation of 406 m was calculated for the 3D model area, and therefore an elevation of -4594 m rsl was used as the bottom of the resource (see Table 1). This average surface elevation is generally lower than the actual elevation in the NW Geysers area where the resource is hottest and thickest, possibly leading to a slight overestimation of the resource in this area.

The total area over which temperature was interpolated was about 3337 km^2, making it the largest of the three areas considered. Within this area a large number of wells with temperature data were available. As described above some of these wells were shallow and constrained the extent of the regional temperature anomaly, but a significant number were deeper than 2000 m and provided good constraints on temperature trends approaching the target region. Most wells show isothermal temperatures in the NTR and were not useful for extrapolation. But wells penetrating below it in the NW Geysers, and throughout the Clear Lake area provided useful conductive gradients. Data for these wells were extrapolated, either individually, or as groups. Published maps of the top of the HTR were also used to constrain shallow temperatures.

Thermal models of intrusion that attempted to match observed heat flow were also used to constrain deep temperatures (Stimac et al., 1997; Norton and Hulen, 2001; Erkan et al., 2005). Temperatures were inferred from Erkan et al. below drilled depths, with some modifications to match extrapolations from wells.

Table 2 summarizes the interpolated temperatures shells at 374°C and above with a base cutoff elevation of 4594 m bsl, and 3D screenshots of the model are shown in Figures 1 to 3. Temperatures range to above 650°C, the solidus of granitic magma. This suggests that a very limited volume of magma or pockets of crystal mush may still be present at drillable depths (Table 2). But by far the highest percentage of the resource is below 500°C. The total rock volume above the critical point was estimated at 228.4 km^3.

Table 2. Interpolated temperature shells and their volumes for the Geysers-Clear Lake area.

Isosurface (°C)	From	To	Volume km3
374	374	400	120.0
400	>400	500	95.4
500	>500	600	11.4
600	>600	650	1.5
650	≥650		0.1
Total	≥374		228.4

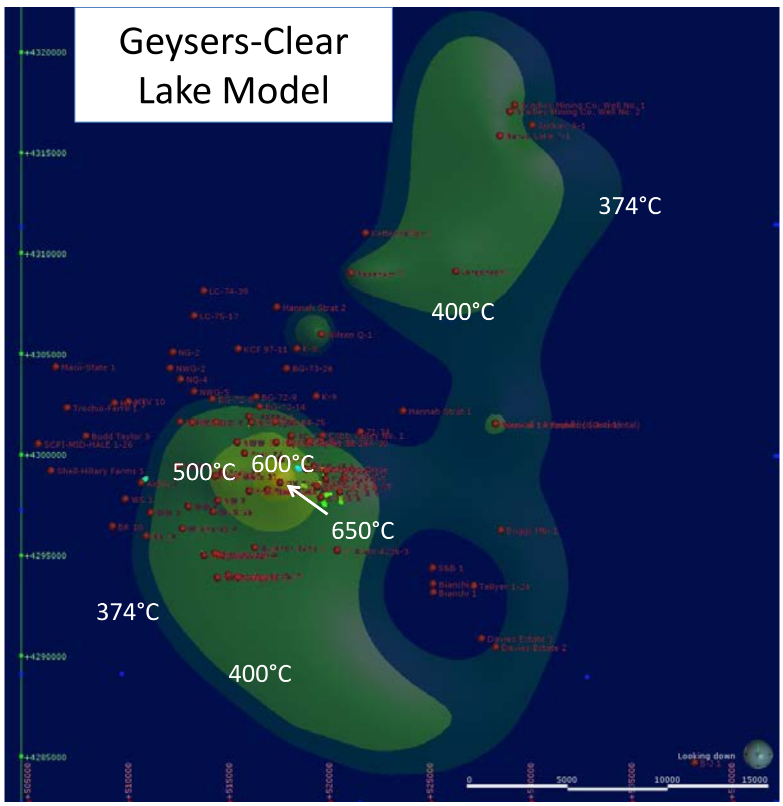

Figure 1. The full temperature model, showing isosurfaces in map view. In this and some subsequent model screenshots, isosurfaces are partially transparent to allow visualization of underlying surfaces. Wells are shown in red. The highest temperatures are predicted in the NW Geysers.

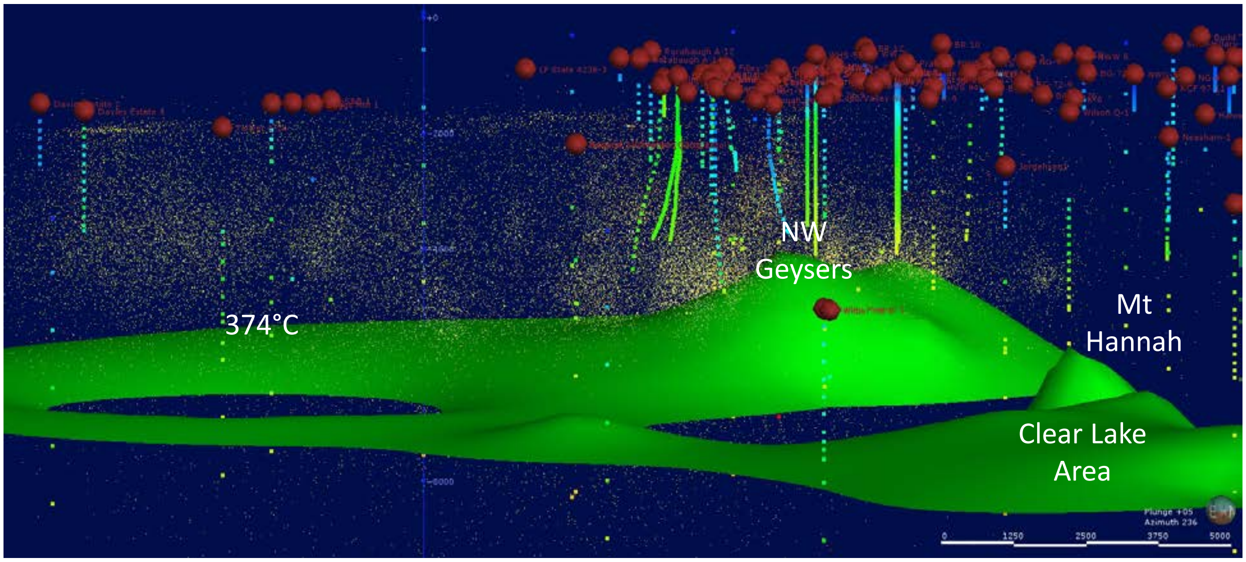

Figure 2. The full temperature model viewed obliquely looking SW, showing the 374°C isosurface (ground surface not shown). MEQs M>1.75 recorded at The Geysers for period 2011-2016. (K. Freeman, Personal Communication, 2017 and LBL Induced Seismicity Website).

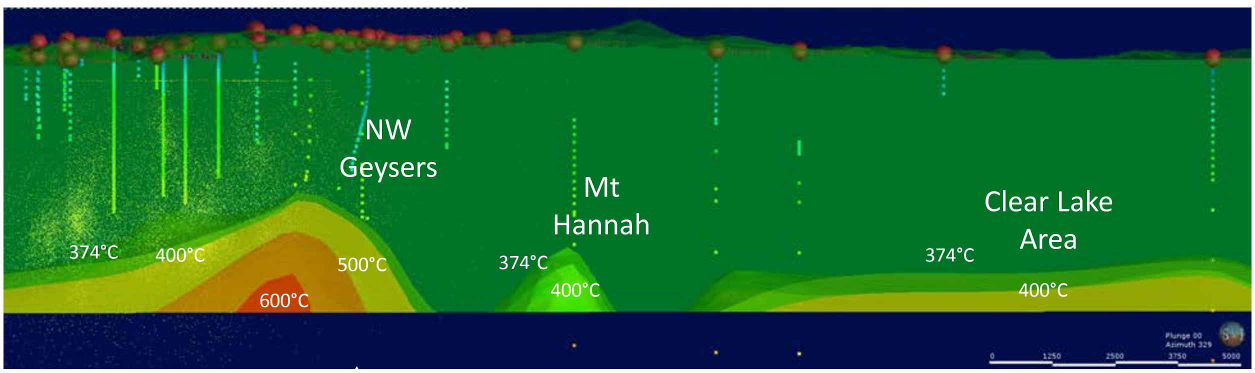

Figure 3. A 5 km-thick vertical slice of the temperature model looking NW and extending from the NW Geysers to the Clear Lake basin. Three prospective areas are evident (NW Geysers, Mt. Hannah, and Mt. Konocti-Borax Lake). MEQs as in Fig. 2. It can be seen that many MEQs lie above the 374°C isotherm, but some also extend below it. This view of the model is truncated at 5 km below average ground surface.

4. The Salton Sea Area

The Salton Sea is one of the ten largest producing geothermal fields in the world, the second largest in the US, and has only been partially exploited due to its very high salinity and partial coverage by the Salton Sea. It has high temperatures and clear magmatic affinities, making it a prime candidate for supercritical geothermal development. On the other hand the fluid chemistry requires extreme measures to reduce corrosion and scaling compared to other fields, and may reduce the effectiveness of hydraulic stimulation. Moreover its high salinity increases the critical point, and thus the depth of the supercritical resource dramatically.

A series of small-volume rhyolite domes were erupted along the rapidly receding shoreline of the Salton Sea. There is also evidence for older rhyolitic volcanism, and mafic dikes present in cuttings from deep wells. Dates of both the exposed and buried rhyolitic volcanics are as young as 2480 ± 470 years (Red Island) (Schmitt et al., 2012).

The conventional Salton Sea geothermal system may be the largest in the US in terms of resource potential, but currently ranks second to The Geysers in terms of current net production of about 340 MWe. The ultimate capacity of the field has been estimated at between 2000 and 2950 MWe (Hulen et al., 2002; Kaspereit et al., 2016). This level of production, if sustainable, would make it the largest capacity geothermal field in the world. The reservoir is one of the most permeable in the world and hosts some of the most prolific geothermal wells drilled (several in the 40-50 MWe range).

4.1 Measured and Interpolated Thermal Gradients

The Salton Sea area has a large number of shallow wells, defining the shape of the shallow thermal gradient in the area (Newmark et al., 1988; Hulen, 2002). Most of these data are from wells drilled to 500 ft or less. It defines the main area of anomalous heat flow in the region, centered on the trend of silicic domes erupted near the southern margin of the Salton Sea. It is possible that the area of anomalously high gradients extends further into the lake, but confirmatory well data are lacking.

Temperature data for numerous deep wells in the Salton Sea area were compiled from the California Division of Oil, Gas, and Geothermal Resources (DOGGR) website to better understand the trends in temperature in and around the Salton Sea geothermal field. A temperature of 390°C was reported for the IID-14 well in the Salton Sea geothermal field (Kaspereit et al., 2016; DOGGR online well records). This well is located on Red Hill, one of the very young rhyolite domes associated with the geothermal system. IID-14 was drilled as an exploration well in 1990 to a depth of 2073 m, and was plugged and abandoned due to the elevated pressures encountered at depth. A number of other wells in the main field reached temperatures of 300-350°C at 3 km or less.

Few significant temperature overturns have been documented in deep wells, even at the margins of the Salton Sea geothermal field. It is more common that deep marginal wells display a more conductive profile that results from lack of permeability at drilled depths, but might also suggest the possibility of a deep convective zone below drilled depths.

4.2 Geophysical Constraints on Magma Bodies and Volumes in the Upper Crust

An extensive MT survey was run over the main Salton Sea field and adjacent lake and numerous resistivity logs were run in wells. Based on the results of this survey, Kaspereit et al. (2006) estimated the field is more than 200 km^2 in area by interpreting the reservoir as having a lower resistivity than surrounding rocks due to the higher temperature and salinity of the fluids. However the publically available MT data do not bear directly on the issue of depth to the brittle-ductile transition zone, or the presence of underlying magma accumulations. A gravity high centered on the silicic domes has been interpreted as evidence of a large underlying mafic intrusion at lower to mid-crustal depths (Biehler, 1964; 1971). In our model we used a version of the gravity data that was obtained from GeoNet, Gravity and Magnetic Dataset Repository. Norton and Hulen (2006) noted that the base of the prominent seismogenic zone lies at about 5 to 6 km depth. They inferred that this is related to magmatic-hydrothermal processes.

4.3 Description of Extent of Supercritical Conditions

The brittle-ductile transition beneath the main Salton Sea field is probably on the order of 4 to 6 km deep based on measured temperatures and patterns of seismicity. Norton and Hulen (2006) inferred pluton tops at about 5.5 km and temperatures of 400-500°C in the region of seismicity, and this inference was accepted and utilized in this study (Figure 5).

It should be noted that the critical point for the Salton Sea field is much higher than for pure water due to its extraordinary salinity. Given that the Salton Sea fluids have extremely elevated salinities of 20-30%, supercritical temperatures would need to exceed 550°C (Driesner and Heinrich, 2007). For the purposes of this study, we will apply the nominal temperature of pure water to the Salton Sea resource evaluation because it likely to roughly correspond with the onset of ductile conditions. However, the enhanced flow properties associated with supercritical fluid might not be as accessible at the Salton Sea as at Coso and The Geysers.

4.4 Estimate of the Extent of the Supercritical Resource

For the Salton Sea area an average ground elevation of -172 ft or -52 m rsl was calculated for the 3D model area, and therefore an elevation of -5052 m rsl was used as the bottom of the resource (see Table 1). This average surface elevation is applicable to essentially the entire resource area.

The total area over which temperature was interpolated was about 600 km^2, making it the smallest of the three areas considered. Within this area a large number of wells with temperature data were available. Some wells are shallow and constrained the extent of the regional temperature anomaly, but a significant number were deeper than 2000 m and provided good constraints on temperature trends approaching the target region. However, temperatures under the lake are only constrained by a few shallow gradient wells, so the supercritical resource could extend further in this direction than modeled.

As discussed earlier, most deep wells in the Salton Sea area show increasing temperatures with depth but are not purely conductive. Exceptions to this are beyond the margins of the developed reservoir (e.g., Fee and Britz wells in the far NE). Therefore extrapolations of temperature profiles have lower confidence. Additionally previously published estimates of temperatures, plastic rock or magma below drilled depths were leveraged into the model (e.g., Norton and Hulen, 2006). The shallowest part of the target region is constrained by highest temperature well at Red Island, and a number of wells in the adjacent Elmore development area. IID-14, the hottest well, was likely drilled within or near recent dikes that fed emplacement of the dome.

Table 3 summarizes the interpolated temperatures shells at 374°C and above with a base cutoff elevation of 5052 m bsl, and 3D screenshots of the model are shown in Figures 4 to 6. Temperatures range to above 600°C, slightly below the solidus of granitic magma, suggesting that no magma is likely present at drillable depths (Table 3). However, the relatively flat surface of the 600°C isotherm indicates that a rather extensive region with pockets of crustal mush might be slightly deeper than the model cutoff. But by far the highest percentage of the resource is below 500°C, and therefore strictly below supercritical conditions based on Salton Sea fluid salinity. The total rock volume of the 374°C shell was the largest of the three areas, estimated at 305.9 km^3.

Table 3. Interpolated temperature shells and their volumes for the Salton Sea area

Isosurface (°C)	From	To	Volume
			km3
374	374	400	107.7
400	>400	500	184.9
500	>500	600	12.7
600	>600	650	0.6
650	≥650		
Total	≥374		305.9

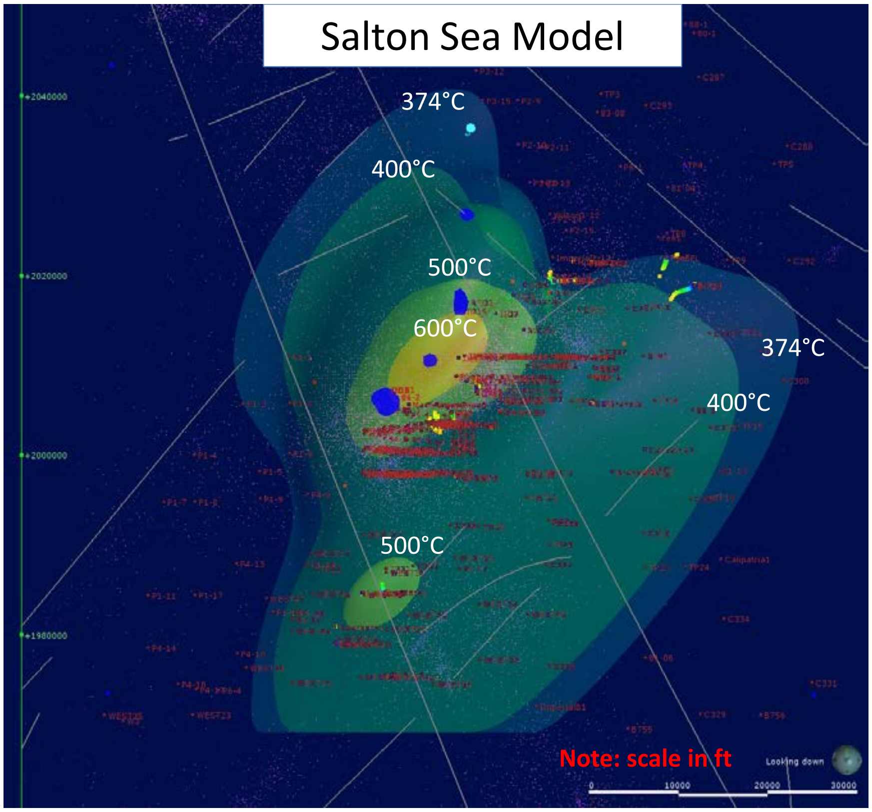

Figure 4. Full 3D model of the Salton Sea in map view showing isosurfaces above the critical point. Rhyolite domes are shown in blue. MEQs as purple dots in this and subsequent images, from 1984 to present from Southern California Earthquake Data Center Website.

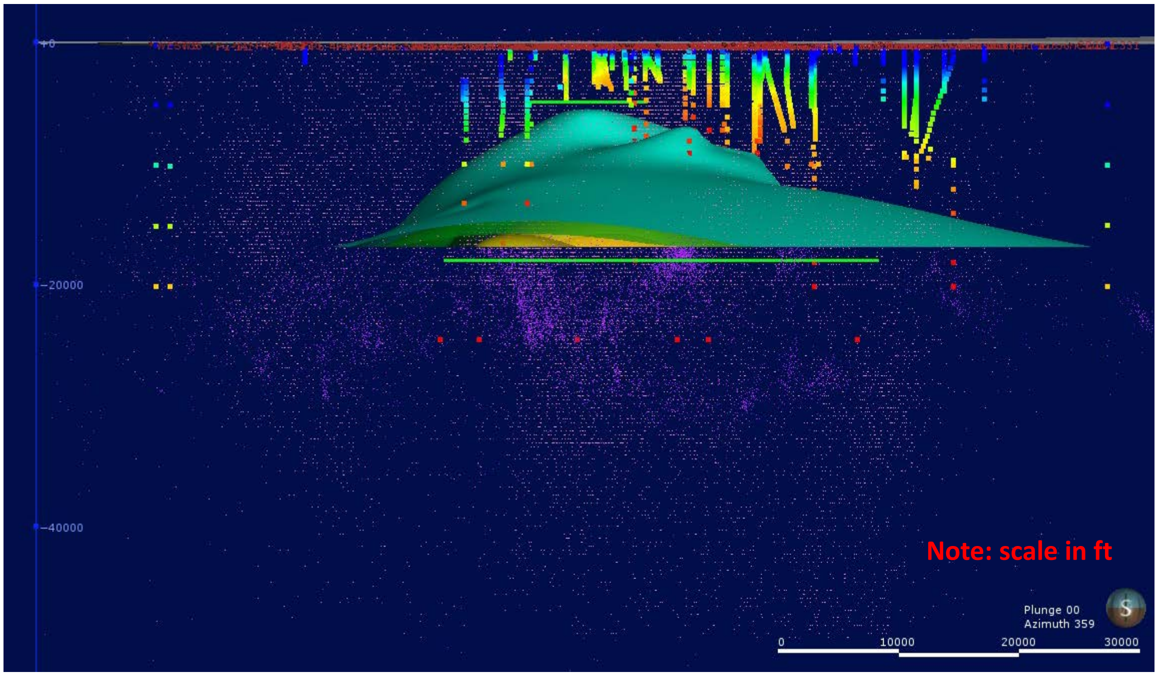

Figure 5. Full 3D model of the Salton Sea showing isosurfaces above the critical point looking N. Well temperatures and temperature control points are color coded points. MEQ density decreases at about the elevation where Norton and Hulen (2006) inferred a magma body.

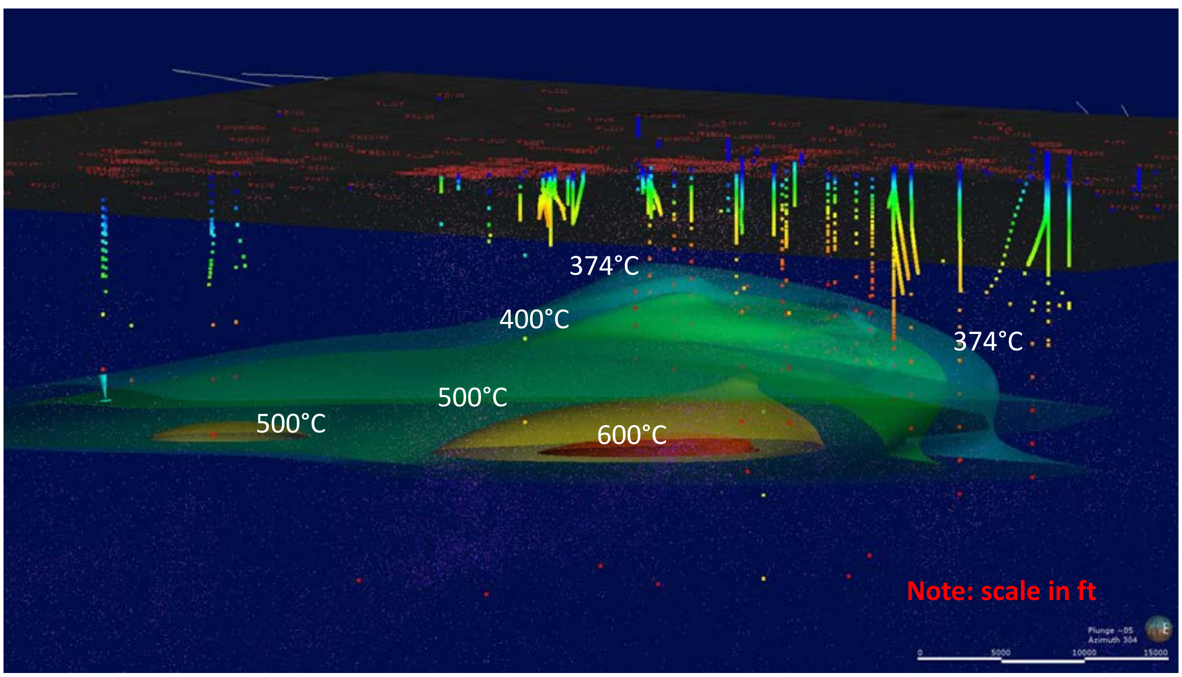

Figure 6. Full 3D model of the Salton Sea showing isosurfaces above the critical point looking WNW. Well temperatures and temperature control points are color coded points.

5. Coso Area

Coso has an installed capacity of 270 MWe, making it the third largest producing geothermal field in the US (Sabin et al., 2015). Production began in 1987, and is now supported by 140 production and injection wells, and facilities that stretch over >10,000 acres (>40 km^2). As described by Sabin et al. (2015, 2016), the resource is owned by the federal government and operated by a third party through a public-private venture contract. It is managed by the Geothermal Program Office (US Navy GPO) and operated by the Coso Operating Company (COC). Commercial power generation began in 1987 (30 MWe) and the field reached its current capacity by the end of 1989.

The two most recent periods of volcanism in the Coso Mountains range from 4.0 to 2.5 Ma and 1.0 Ma to present (Simon et al., 2009). The areal extent of the Coso geothermal field is closely represented by the mapped extent of the Coso volcanic field, and in particular the extent of the youngest rhyolite domes. The heat source is interpreted as a silicic magma chamber with its top as shallow as 5 km. Frequent seismicity (Walter and Weaver 1980), as well as teleseismic P-delay tomography (Reasenberg et al., 1980) provides evidence for a magma body with a current estimate for the top of the body at ~5 km below the surface (Wilson et al., 2003). An associated upwarping of the brittle-ductile zone lies directly beneath the Coso geothermal field and as shallow as 4 km (Wicks et al., 2001; Unruh et al., 2002a, b; Monastero et al., 2005).

5.1 Measured and Interpolated Thermal Gradients

The Coso thermal anomaly was originally delineated by the distribution of thermal features, hydrothermal alteration, and shallow gradient wells (Combs, 1980). The thermal anomaly is nearly coincident with the location of Pleistocene rhyolite domes occupying a north-trending structural and topographic ridge. Temperatures were measured in 25 shallow and 1 intermediate depth borehole, with geothermal gradients ranging from 25.3°C/km to 906°C/km. The high gradients were related to a convecting geothermal system currently supplying production (Combs, 1980). Unruh et al. (2004) lists five deep wells that encountered temperatures over 300°C. They inferred based on these wells that the 350°C isotherm is probably reached by about 4 km depth at Coso.

5.2 Geophysical Constraints on Magma Body Locations and Volumes in the Upper Crust

The Coso volcanic field is one of the most seismically active regions in the United States, producing on average about 20 earthquakes/day although more than 80% of these are at magnitudes (M) <1.0 (Lees, 2002; Kaven et al., 2011; Sabin et al., 2015). Ongoing investigations are designed to possibly differentiate between induced and tectonic seismicity, including potential correlation of field-wide activities with variations in seismic moment release (e.g., Kaven et al., 2013, 2014).

Zhang and Lin (2014) used 3-D high-resolution Vp and Vp/Vs models to identify an anomalous low-velocity body underlying the Coso geothermal field at depths of 6 to 12 km. This feature was interpreted to represent ductile rock associated with a mostly crystallized silicic intrusion, but is not likely to include pervasive partial melt due to a lack of high Vp/Vs ratios. It is more consistent with a crystal mush zone or column with a small percentage of melt.

Lees (2002) interpreted anomalies in seismic velocity, attenuation, and anisotropy, as well as stress, in the southwestern part of the Coso field. The anomalies also correlated with high heat flow in the field and the termination of geothermal production to the south. He speculated that the top of an intrusion is present in this region at 3-4 km bsl that causes significant perturbation of stress in the field (Lees, 2002).

5.3 Estimate of the Extent of the Supercritical Resource

Minimal measured temperature data in deep wells were available for Coso. Well data is considered confidential on DOGGR, and was not generally available from the operators, with the exception of a handful of deep wells. These were supplemented by published well profiles, contoured maps, and interpolations were available. A 3D temperature interpolation was created using these sources and reasonable boundary conditions at the model margins. In particular the western side of the field was modeled by incorporating the higher temperature portion of a model (Sabin et al., 2016) created for the U.S. DOE’s FORGE EGS evaluation by D. Siler (USGS). The grid of interpolated FORGE temperatures was obtained from the Geothermal Data Repository Website.

5.4 Permeability Constraints

The expected supercritical region beneath the Coso reservoir has already been described by Unruh et al. (2004), Unruh and Hauksson (2005), Hauksson and Unruh (2007), and Rose et al. (2012), among others. Rose et al. (2012) summarized the expected state of fracturing and permeability as follows:

“As temperature increases with depth and proximity to the heat source, crystal plastic deformation becomes the dominant means of accommodating strain. Large earthquakes can locally extend the depth of micro-seismicity by locally increasing the strain rate. However, the permeability of fault and country rock in this zone is expected to be quite low.”

5.5 Resource Extent

For Coso an average ground elevation of 1100 m asl was calculated for the 3D model area, and therefore an elevation of 3900 m bsl was used as the bottom of the resource (see Table 1).

The total area over which temperature was interpolated was about 852.5 km^2, making it the second largest of the three areas considered. Within this large area only a few deep wells with temperature data were available. Shallow heat flow and previous interpolations of deep wells were also considered. However, the primary constraints on deep temperatures were several previous interpretations of the depth to the brittle-ductile transition, and MEQ locations from the Southern California Earthquake Data Center Website. Table 4 summarizes the interpolated temperature shells at 374°C and above with a base cutoff elevation of 3900 m bsl and 3D screenshots of the model are shown in Figures 7 to 9. Temperatures range to between 374°C and 500°C, well below the solidus of granitic magma, indicating that no magma is likely present at drillable depths (Table 4, Figs. 7- 9). The total rock volume above the critical point was estimated at 16.6 km^3. This is much smaller than the other fields, which are truly exceptional in their extent. The supercritical resource at Coso appears to lie mostly below 5 km bsl, and thus may await technological advances that allow ultradeep drilling.

Table 4. Interpolated temperature shells and their volumes for the Coso area.

Isosurface (°C)	From	To	Volume
			km3
374	374	400	13.8
400	>400	500	2.8
500	>500	600	
600	>600	650	
650	≥650		
Total	≥374		16.6

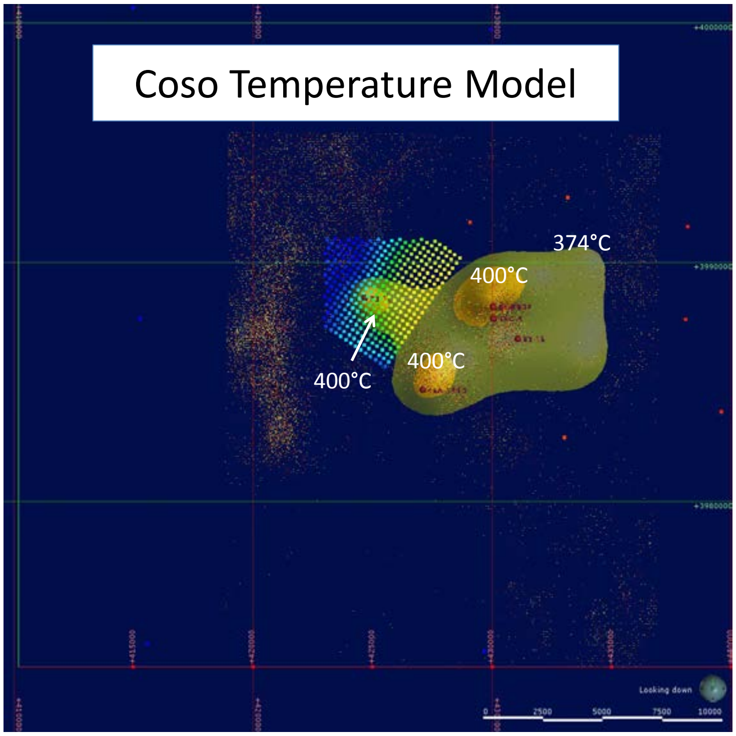

Figure 7. The Coso model with major isosurface seen in map view, the temperature interpolation from West Flank FORGE model (D. Siler, Personal Communication, 2017, Geothermal Data Repository Website), deep wells (red), and MEQs (yellow to red dots).

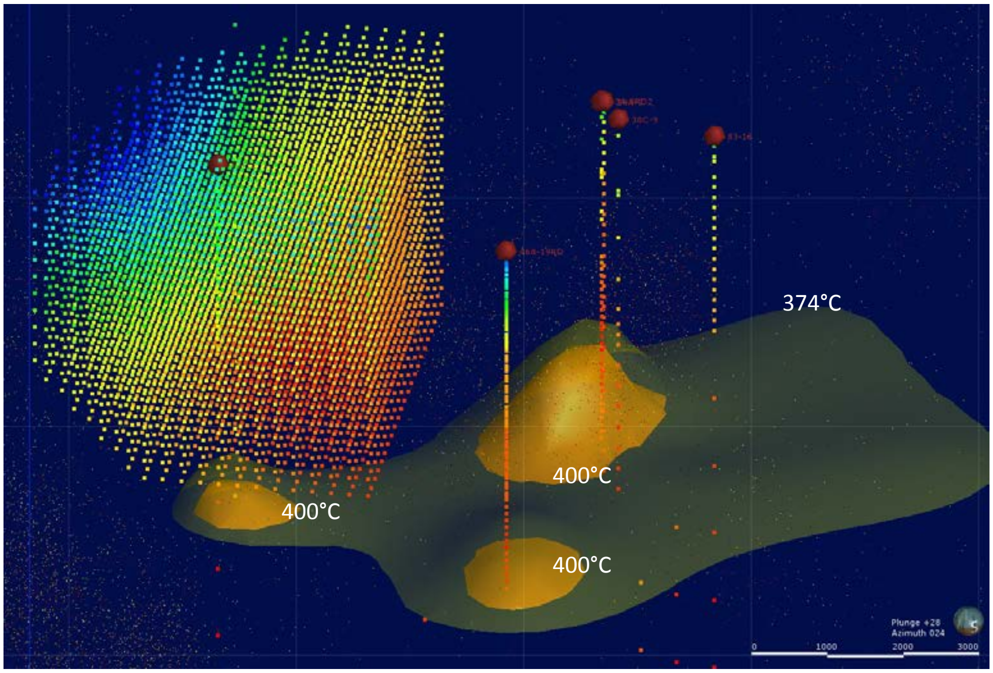

Figure 8. The Coso model viewed obliquely looking NNE. The temperature interpolation from West Flank FORGE model (gridded points), deep wells temperatures and extrapolation (color coded points), and MEQs (yellow to red dots).

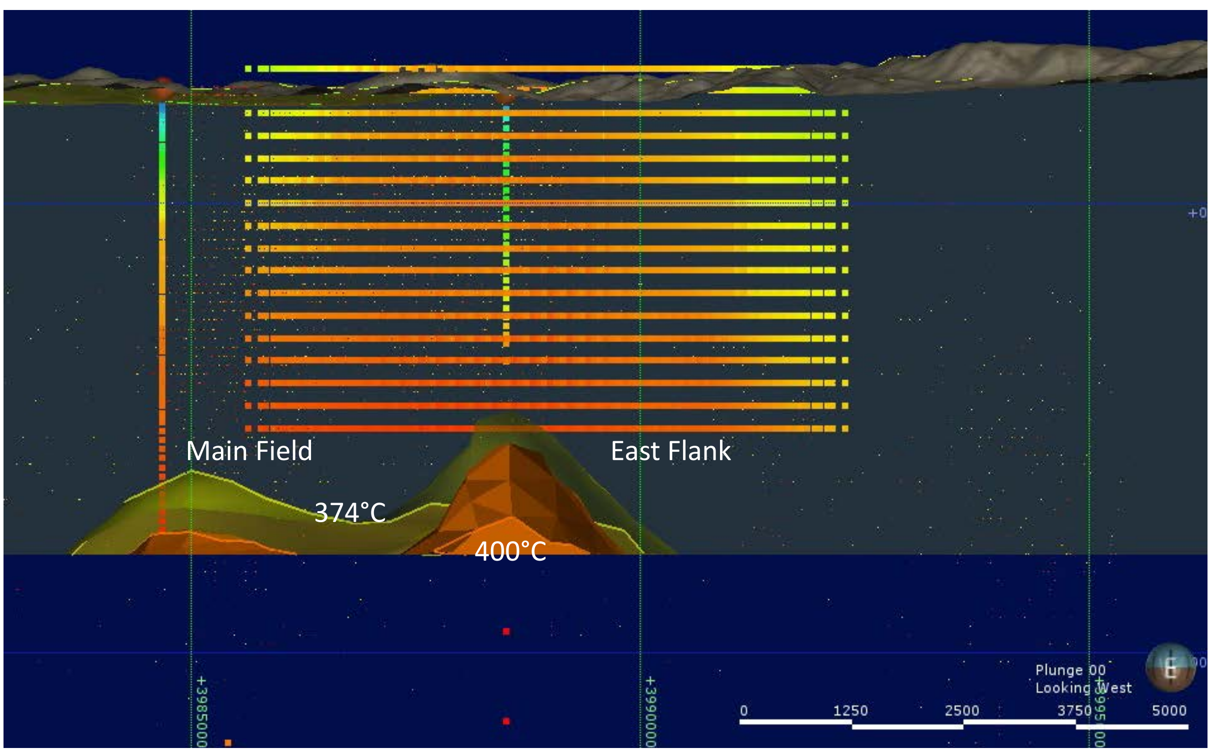

Figure 9. The Coso model looking W, the temperature interpolation from West Flank FORGE model (gridded points) deep well temperatures (color coded points), and MEQs (yellow to red dots).

6. Supercritical Resource Capacity Estimates (MWe)

Now that we have made volumetric estimates of supercritical rock volumes in each field we proceed to estimate their MWe power production capacity. Such volumetric assessment of geothermal resources has traditionally been performed for exploration prospects using a variety of methods including power density, natural heat loss, stored heat (heat-in-place), and numerical modeling (Benoit, 2013; Grant and Bixley, 2011). The most robust resource capacity estimates are made using a 3D numerical model of the reservoir, coupled to wellbore models of the production and injection wells, and informed by extensive and detailed geoscientific data (Wilmarth and Stimac, 2015). However, given the very large uncertainties in the extent of supercritical resources and how they may be produced, sophisticated numerical modeling of resource capacity seems inappropriate. In this study the volumetric heat capacity (heat-in-place) and power density methods are used to assess the resource capacity of The Geysers, Salton Sea, and Coso.

One common volumetric heat capacity method estimates reasonable ranges of resource area, thickness, porosity, and temperature to calculate a range of volumetric heat-in-place results, then applies a recovery factor and power plant efficiency to estimate the amount of electrical energy that might be practically generated from the total heat-in-place. The recovery factor is intended to account for the characteristics governing reservoir heat extraction including permeability, flow patterns, and temperature distribution based on a simple heat-sweep model of a broadly permeable reservoir. The most elaborate of the heat-in-place techniques uses the Monte Carlo method to apply triangular parameter distributions to calculate a population of possible heat energy contents in the reservoir based on reasonable ranges of the parameters (Sanyal and Sarmiento, 2005; Williams, 2014).

The heat-in-place approach assumes that the limiting factor associated with operating capacity will be well decline and eventual shut-down due to cooling from re-injection. However experience shows that capacity limits are also often associated with water availability, surface access, pressure interference, events such as cold water invasion from outside the reservoir, and economics of the power market. Many of the detrimental reservoir processes may be mitigated through proactive field management. Furthermore, recognition of production-related cooling in production wells is known to occur but generally does not dominate production well fields, partly since it is likely to be a late stage phenomenon (Grant, 2015). Considering the variety of mechanisms that limit capacity, it is misleading and often inappropriate to calculate capacity based on a simplistic cooling model.

6.1 Permeability and Recovery Factor

Conventional geothermal systems typically have a high permeability fracture network, and the presence of a working fluid. Early resource estimates for conventional geothermal systems using the heat-in-place method used a recovery factor of 25%. Grant and Bixley (2011) reviewed the application of recovery factors for conventional geothermal systems, and found that they have generally been overestimated, sometimes by a factor of 5 or more. Grant and Bixley (2011) concluded that for most conventional systems a recovery factor on the order of 10% was reasonable, but that it “could be larger or smaller by a factor of two” (i.e., 20% to 5%, with 10% as the most likely case).

It would be expected that recovery factors appropriate for Supercritical Geothermal Resources (EGS) in an unstimulated state would be lower than for conventional naturally fractured systems, as the fractures of EGS systems will very likely have smaller aperture and be less pervasive, or be completely absent. As described above, the general condition of conductive temperature gradients is consistent with permeability below the threshold to support convection, and the absence or scarcity of a working fluid.

Systems in an active state of magmatic fluid expulsion could certainly have natural fluid circulation as described by Fournier (1991, 1999) as illustrated by porphyry and deep shear zone ore deposits (Cox, 2005), but the likelihood of encountering such a condition is deemed low in the systems being reviewed, again with the possible exception of the Salton Sea.

Typical liquid systems show declines in permeability with depth and limited areas of liquid upflow. Targeting the immediate vicinity of upflow zones might increase the probability of encountering natural permeability even at critical conditions, but otherwise it is likely stimulation would be required to access stored heat at economic rates.

Certainly the most likely case is that recovery of heat from a ductile rock mass would be lower than a conventional brittle one without some assistance from hydraulic fracturing. In fact even in conventional reservoirs there is evidence that permeability generally declines with depth (Bottomley and Grant, 1998), and this is the general trend observed in the crust (e.g., Ingebritsen and Manning, 2010).

Most EGS schemes entail hydraulic stimulation to re-activate and open existing sealed fractures, and inject a working fluid to mine heat along the fracture path. This effectively increases the local permeability of the system as long as fluid is pumped through the fracture network. One applicable example of a supercritical EGS system would be the Demonstration Project in the NW Geysers (Garcia et al., 2012, 2016). In this example, fluid is injected into the steam reservoir through deep wells, and falls by gravity along steam-saturated fractures to the base of the permeable fracture network. There is evidence that the fracture network extends much deeper than drilled productive reservoir, and that some stimulation of sealed or partially sealed fractures occurs as the result of injection of cold water. At the NW Geysers, a progressive deepening of microseismic events over time (~100m/y) was observed in the vicinity of injection wells, suggesting that injection of cold water has resulted in enhanced permeability at depth (Jeanne et al., 2016). One might expect that the recovery factor applied to steam systems might be higher than to liquid systems due to the potentially more effective placement of injected fluids.

Grant (2016) provided a recent review of the use of recovery factors in EGS, noting that data from existing EGS and HDR projects have recovery factors ≤ 2 %. These values are significantly lower than those recommended for conventional hydrothermal fields, which typically average 10% as described above (Williams, 2007; Grant and Bixley, 2011). Grant (2016) suggests that multi-zonal stimulation, which has been employed for unconventional petroleum resources, or a similar method, will be required to create more pervasive permeability in future EGS reservoirs, leading to higher recovery factors.

For EGS systems microseismicity related to injection may indicate significant reservoir volumes stimulated by fracturing, but the reservoir developed through seismic action may be markedly smaller than the extent of seismicity (Williams, 2010; Grant and Garg, 2012). Grant (2015) concluded that “as with hydrothermal systems, it appears that modelling studies have erred on the optimistic side, but for EGS by an even greater amount. Recovery factors for EGS should be at best a few percent. The theoretical estimates have assumed uniform or random fracturing. It can be observed that in practice the fracture system is neither uniform nor random. Instead there is a single plane of fracturing, with permeability that is effectively swept by fluid extending only a small distance away from the plane.”

For the Salton Sea, the high salinity of the deep reservoir may make it difficult for injected low density fluid to effectively move downward. On the other hand this system has perhaps the highest natural permeability of any major geothermal system on Earth due to the nature of the reservoir rock and the operative tectonic processes. Therefore it is considered that average bulk permeability may be higher. In our estimates we consider that these two countervailing trends, high salinity and high natural permeability, may approximately cancel each other out and therefore we use the same range of recovery factors for the Salton Sea as for the other two fields. A more accurate assessment of their relative importance awaits actual field pilot tests.

In general recovery factors should scale with the average permeability of the rock mass. Impermeable rock would have a recovery factor near 0 unless permeability could be stimulated and maintained. Conventional geothermal reservoirs with average permeability should equate to the 5% to 20% range discussed above. For unconventional reservoirs there is very little actual experience to constrain recovery factors. In this study we employed a range of thermal recovery factor from 0.1% to 4%.

6.2 Heat-in-Place Estimates

6.2.1 Inputs

Resource capacity for the three fields was estimated using a proprietary heat-in-place model and based on the method described in Garg and Combs (2015). The input parameters for the heat-in-place model are organized into two groups as shown in Table 5. The Group 1 parameters are specified using resource data and the Group 2 parameters are based on economic and engineering considerations for a typical flash cycle power plant. The input parameters with a maximum, minimum, and a most likely value were modelled with a triangular probability distribution. Parameters with only a maximum and minimum were modeled with a uniform probability distribution.

The temperature models for each field were divided into four volumetric shells determined from 3D interpolation of temperature in Leapfrog models. Each shell was evaluated for resource capacity separately, and then summed. The four shells are 374-400°C, 400-500°C, 500-600°C, and 600-650°C. Reservoir depth for each temperature shell was chosen based on the depths of the temperature shells evaluated from the Leapfrog models. The middle temperature for the triangular distribution was chosen as the mean of each shell’s temperature range.

Table 5. Generalized input parameters for heat-in-place model.

Heat-in-Place Input Parameters				
Group 1 input parameters	units	min	middle	max
Reservoir Volume	km^2	-	$V_{(T2-T1)}$	-
Reservoir Depth	m	Z_1	Z_2	5000
Reservoir Temperature	deg C	T_1	$0.5*(T_2-T_1)$	T_2
Thermal Recovery Factor	fraction	0.001	-	0.04
Group 2 input parameters	units	min	middle	max
Volumetric Heat Capacity	kJ/m^3-K	2700	-	2700
Separator Temperature	°C	165	-	165
Condenser Temperature	°C	40	-	40
Conversion Efficiency	fraction	0.7	-	0.8
Plant or Project Life	years	30	-	30
Plant Load Factor	fraction	0.90	-	0.97

Note: Inputs and calculations after Garg and Combs (2015).
- = value either not required or not used for distribution calculations.
T_2 = Upper temperature of shell
T_1 = Lower temperature of shell
$V_{(T2-T1)}$ = Reservoir shell volume between T_2 and T_1
Z_1 = Minimum Depth to T_1
Z_2 = Depth to approximate maximum volume of shell T_2 - T_1

Thermal recovery factor was chosen as a range from 0.1% to 4% based on the preceding discussion. The low end of this range (0.1%) corresponds to the pessimistic case representing scenarios with extremely low natural permeability and unsuccessful reservoir stimulation. The higher end of the range (4%) corresponds to low natural permeability reservoir rocks typical of the conditions at the depth of these supercritical resources coupled with successful hypothetical reservoir stimulation efforts that are able to increase bulk permeability to levels similar, but still somewhat less than the lower range of natural geothermal reservoir permeability (~5%). We consider this range reasonable using current reservoir stimulation technologies and unlikely to grossly overestimate the resource capacity. The same recovery factor ranges were used for all three fields because simply too little is definitively known to fine-tune the ranges at this time.

A total of 10,000 iterations of the Monte Carlo simulation were completed for each temperature shell. The outcome populations are expressed in megawatts of electrical power generation (MWe) over the project life. The results of the statistical evaluation are summarized below, with a percent confidence assigned for each MW estimate, where 90% (P90) confidence represents a conservative estimate and 10% confidence (P10) represents an optimistic estimate.

6.3 The Geysers-Clear Lake

Model results for The Geysers-Clear Lake area are shown in Table 6 and span a range of power capacities from 215 MW to 1585 MW with a P50 value of 890 MW. For reference, this P50 value is similar to the current capacity of the conventional steam reservoir, and about half of the maximum capacity of the field over its nearly 60 year production history.

Table 6. Resource input parameters and output capacities from supercritical heat-in-place model of The Geysers-Clear Lake.

THE GEYSERS

Shell (°C)	Reservoir Depth (m)			Volume
	Minimum	Middle	Maximum	(km^3)
374-400	2250	4500	5000	120.0
400-500	2500	4500	5000	95.4
500-600	3000	4500	5000	11.4
600-650	4000	4500	5000	1.5
Total				228.4

MWe Capacity		
Percent Confidence		
90%	**50%**	**10%**
96.6	403.3	713.8
100.2	409.5	734.8
16.3	66.9	118.3
2.4	10.4	18.5
215.5	890.2	1585.5

6.4 Salton Sea

Model results for Salton Sea are shown in Table 7 and span a range of power capacities from 304 MW to 2204 MW with a P50 value of 1259 MW. For reference, this P50 value is more than triple the field's current capacity and similar to some estimates of the conventional reservoir's maximum capacity (Hulen et al., 2006; Kaspereit et al., 2016).

Table 7. Resource input parameters and output capacities from supercritical heat-in-place model of the Salton Sea.

SALTON SEA

Isosurface (°C)	Reservoir Depth (m)			Volume
	Minimum	Middle	Maximum	(km^3)
374-400	1000	4500	5000	107.7
400-500	1500	4500	5000	184.9
500-600	3000	4500	5000	12.7
600-650	4250	4500	5000	0.6
Total				305.9

MWe Capacity		
Percent Confidence		
90%	**50%**	**10%**
86.8	363.2	645.4
198.1	816.8	1419.9
18.5	75.1	131.5
1.0	4.2	7.5
304.5	1259.3	2204.3

6.5 Coso

Model results for Coso are shown in Table 8 and span a range of power capacities from 14 MW to 2104 MW with a P50 value of 59.2 MW. For reference, this P50 value is significantly less than the field's current capacity. The relatively low estimate is due primarily to the relatively deep top on the supercritical resource, which mostly lies below the 5 km depth cutoff considered here.

Table 8. Resource input parameters and output capacities from supercritical heat-in-place model of Coso.

COSO

Isosurface (°C)	Reservoir Depth (m)			Volume
	Minimum	Middle	Maximum	(km^3)
374-400	500	4500	5000	13.8
400-500	1000	4500	5000	2.8
Total				16.6

MWe Capacity		
Percent Confidence		
90%	**50%**	**10%**
11.0	47.0	82.4
3.0	12.2	21.5
14.0	59.2	104.0

6.6 Power Density Estimates

Power density estimates can serve as a simple check on heat in place estimates as they rely on fewer assumptions and are calibrated against a large number of known operating fields (Wilmarth and Stimac, 2015). Power density estimates were made for the three regions detailed in this study using the log-normal worksheet provided by Cumming (2016). Resource areas were calculated from the 374°C contour at a depth of 5 km. Power densities were chosen by projecting the trends between reservoir temperature and power density described in Wilmarth and Stimac (2015) to higher temperatures. A pessimistic (P90) power density of 5 MW/km^2 and an optimistic (P10) value of 100 MW/km^2 were projected from the main trends in Figure 10. The log-normally derived P50 value for power density from this range is 22 MW/km^2, similar to the typical values for conventional liquid-dominated systems on the "Main Sequence" at ~300°C.

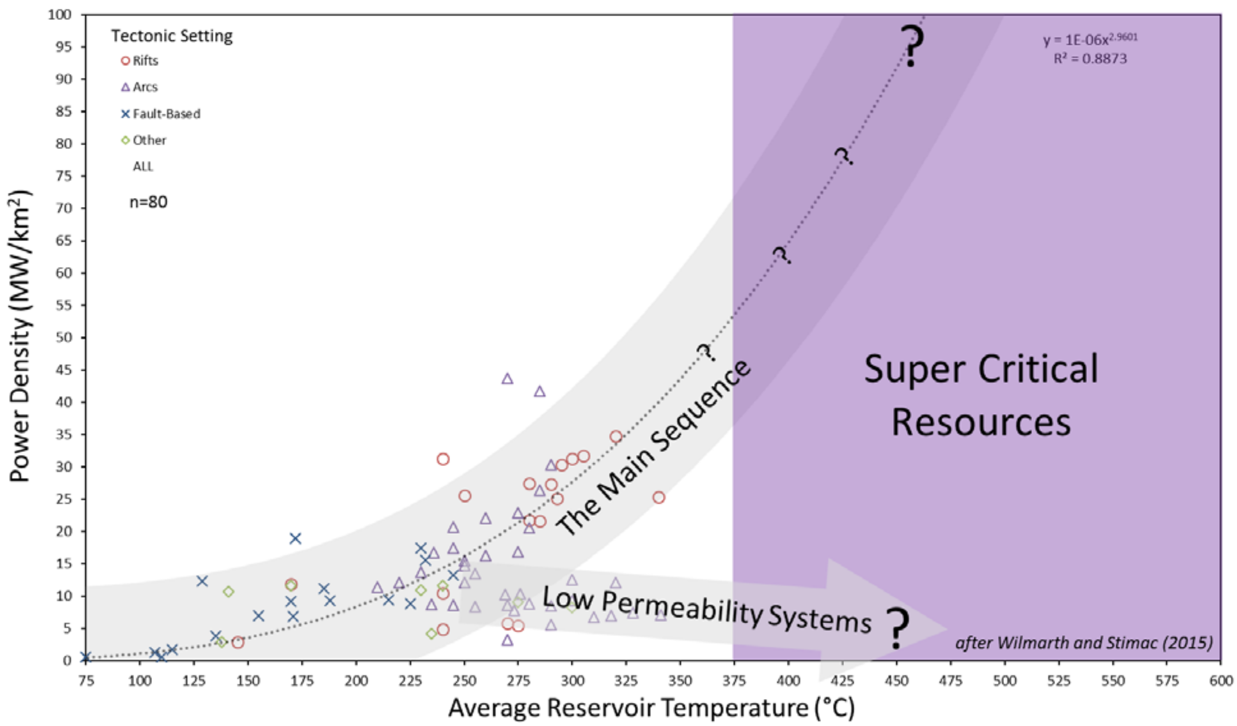

Figure 100. Power Density vs Average Reservoir Temperature for 80 operating fields with trends extrapolated to supercritical temperatures.

This calculation results in a very wide range of potential power capacities for the three fields, ranging from hundreds to tens of thousands of MWs. This large range results from the lack of information about producing supercritical resources and the corresponding poorly constrained resource parameters. Since power density estimates do not consider depth to resource it is likely this method is not very suitable for accurate estimation of deep supercritical resources. The appropriate values for power density are likely to be on the lower end of the range used here.

Even so, the overlap of the heat-in-place estimates with the lower end of the power density estimates gives some confidence in the values for resource capacity calculated. The middle range values of the heat-in-place capacity estimates suggest that correlating the two methods would require corresponding power density numbers of ~2-3 MW/km^2, which is a low number for a conventional geothermal system. We consider that with current technologies the lower estimates are likely to be closer to the actual supercritical resource capacities.

7. Estimate of the Overall US Supercritical Resource Base

A recent update of the EGS potential of the US was based on areas with temperatures exceeding 150°C and depths between 3 and 7 km (Augustine, 2016). The regions of anomalous temperature are based on revised maps from Southern Methodist University (SMU) by Blackwell et al. (2011). The EGS potential is estimated at 5157 GWe, a net increase of 925 GWe over previous estimates (Augustine, 2011) over the same depth range, but lower than the estimate to 10 km depth of 16,000 GWe. The estimate is based on heat-in-place, a decline in reservoir temperature of 10°C, and assuming a recovery factor of 20% on that increment. We note that the 20% recovery factor only applies to the assumed 10°C temperature drop. The net effect of this methodology is to cool the reservoir by 2°C. The EGS resource per km^3 of rock exceeding 350°C was estimated at 1.19 MWe (Augustine, 2016). A previous study by Augustine (2011) to 10 km accounted for 79,540 MWe of EGS resource with temperatures >350°C in the conterminous U.S., mostly located from 8 to 10 km depth.

We note that the SMU maps intentionally screened out high heat flux in and around existing hydrothermal sites. In contrast, our study looked specifically at some of these sites in detail. Thus it is not surprising that our estimated supercritical resource from the three largest geothermal fields in the US to a depth of about 5 km exceeds the equivalent temperature EGS resources by a broad margin (Augustine, 2016). Furthermore we would expect a significantly larger resource to 7 km if we had evaluated it. As an example, a detailed evaluation of the Cascades region has resulted in higher estimates of EGS resources (Frone et al. 2015). Our work is consistent with this and strongly suggests that detailed, regional or site-specific resource estimates will result in identification of more supercritical EGS than previously thought to exist.

ACKNOWLEDGMENTS

This work was supported by the U.S. Department of Energy's Geothermal Technologies Office, under Contract No. 1784593. Many thanks to Eric Hass and Holly Thomas for their assistance. Amanda Fishbin and Ian Haizlip (Geologica Geothermal Group) are thanked for help with data compilation and resource capacity calculations. Mark Walters (Calpine) was very gracious in sharing ideas and making critical data available for the Clear Lake-Geysers area. Ole Kaven (U.S. Geological Survey) provided assistance with access to earthquake data, Jess McCulloch (Terra-Gen Operating Company) provided key temperature data for deep wells, and Kelly Blake and Andy Sabin (U.S. Navy) provided guidance on published data sources for Coso. Katie Freeman (LBNL) provided seismic data from The Geysers catalog through the Induced Seismicity Data Website at the Lawrence Berkeley National Laboratory, which is supported by the U.S. DOE Geothermal Technologies Office. Drew Siler (U.S. Geological Survey) shared ideas and interpretations made for the West Flank FORGE area of Coso.

REFERENCES

American Oil and Gas Historical Society, 2017, Anadarko Basin in depth, Webpage accessed 30-April-2017. http://aoghs.org/editors-picks/anadarko-basin-depth/

Augustine, C., 2011, Updated U.S. Geothermal Supply Characterization and Representation for Market Penetration Model Input. National Renewable Energy Laboratory Report TP-6A2-47459, 89 p.

Augustine, C., 2016, Update to Enhanced Geothermal System Resource Potential Estimate. GRC Trans. 40, 673-677.

Beall, J.J., Wright, M.C., 2010, Southern extent of The Geysers high temperature reservoir based on seismic and geochemical evidence. GRC Trans. 34, 1199-1202.

Benoit, D., 2013, An Empirical Injection Limitation in Fault-Hosted Basin and Range Geothermal Systems, GRC Trans. 37, 887-894.

Biehler, S., 1964, Geophysical study of the Salton Trough of southern California. Pasadena, Calif., California Institute of Technology, Ph.D. Thesis, pp. 1-139

Biehler, S., 1971, Gravity studies in the Imperial Valley. In: Cooperative Geological-Geophysical-Geochemical Investigation of Geothermal Resources in the Imperial Valley Area of California, University of California, Riverside, Education Research Service, report dated July 1, 1971, pp. 1-154.

Blackwell, D., Richards, M., Frone, Z., Batir, J., Ruzo, A., Dingwall, R., Williams, M., 2011, Temperature-at-Depth Maps for the Conterminous U.S. and Geothermal Resource Estimates. GRC Trans. 35, p. 1545-1550.

Combs, J., 1980, Heat flow in the Coso Geothermal Area, Inyo County, California. J. Geophys. Res. 85, 2411-2424.

Cox, S.F., 2005, Coupling between deformation, fluid pressure, and fluid flow in ore-producing hydrothermal systems at depth in the crust. Econ. Geol. 100th Anniversary Volume, 39-79.

Cumming, W., 2016, Resource Capacity Estimation Using Lognormal Power Density from Producing Fields and Area from Resource Conceptual Models; Advantages, Pitfalls and Remedies, Proceedings 41st Workshop on Geotherm. Res. Eng. Stanford University, SGP-TR-209.

Dobson, P., Asanuma, H., Huenges, E., Poletto, F., Reinsch, T., Sanjuan, B., 2017, Supercritical Geothermal Systems – A Review of Past Studies and Ongoing Research Activities. Proceedings 41st Workshop on Geotherm. Res. Eng., Stanford University, SGP-TR-212.

Donnelly-Nolan, J.M., Hearn, B.C., Jr., Curtis, G.H., Drake, R.E., 1981, Geochronology and evolution of the Clear Lake volcanics, U.S. Geological Survey Professional Paper 1141, 47–60.

Driesner, T., Heinrich, C.A., 2007, The system H_2O–NaCl. Part I: Correlation formulae for phase relations in temperature–pressure–composition space from 0 to 1000°C, 0 to 5000 bar, and 0 to 1 XNaCl, Geochim. Cosmochim. Acta, 71, 4880-4901.

Elders, W.A., Friðleifsson, G.O., Albertsson, A., 2014, Drilling into magma and the implications of the Iceland Deep Drilling Project (IDDP) for high-temperature geothermal systems worldwide. Geothermics 49, 111-118.

Erkan, K., Blackwell, D.D., Leidig, M., 2005, Crustal Thermal Regime at The Geysers/Clear Lake area, California. Proceedings World Geothermal Congress 2005.

Fournier, R.O., 1991, The transition from hydrostatic to greater than hydrostatic fluid pressure in presently active continental hydrothermal systems in crystalline rock, Geophys. Res. Letters, 18(5), 955-958.

Fournier, R.O., 1999, Hydrothermal processes related to movement of fluid from plastic into brittle rock in the magmatic-epithermal environment. Econ. Geol. 94, 1183-1211.

Friðleifsson, G.O., Albertsson, A., Stefansson, B., Gunnlaugsson, E., and Adalsteinsson, H., 2007, Deep unconventional geothermal resources: a major opportunity to harness new sources of sustainable energy, Proceedings, 20th World Energy Conference, Rome, World Energy Council, 21 p.

Friðleifsson, G.O., Elders, W.A., Albertsson, A., 2014, The concept of the Iceland deep drilling project. Geothermics 49, 2-8.

Frone, Z., Richards, M., Blackwell, D., and Augustine, C., 2015, Shallow EGS resource potential maps of the Cascades. Proceedings 40th Workshop on Geothermal Reservoir Engineering, Stanford University. SGP-TR-194, 15 p.

Garcia, J., Walters, M., Beall, J., Hartline, C., Pingol, A., Pistone, S., and Wright, M., 2012, Overview of the Northwest Geysers EGS demonstration project. Proceedings 37th Workshop on Geothermal Reservoir Engineering, Stanford University. SGP-TR-194.

Garcia, J., Hartline, C., Walters, M., Wright, M., Rutqvist, J., Dobson, P.F., Jeanne, P., 2016, The Northwest Geysers EGS Demonstration Project, California Part 1: Characterization and reservoir response to injection, Geothermics, 63, 97-119.

Garg, S.K., Combs, J., 2015, A reformulation of USGS volumetric “heat in place” resource estimation method. Geothermics, 55, 150-158.

GeoNet, Gravity and Magnetic Dataset Repository. http://irpsrvgis00.utep.edu/repositorywebsite/

Geothermal Data Repository Website. https://gdr.openei.org/home

Grant, M.A., 2015, Resource Assessment, a review, with reference to the Australian Code, Proceedings World Geothermal Congress 2015, 6 p.

Grant, M.A., 2016, Physical performance indicators for HDR/EGS projects. Geothermics 63, 2-4.

Grant, M.A., Bixley, P.F., 2011, Geothermal Reservoir Engineering. 2nd Ed., Academic Press (Elsevier), 359p.

Grant, M.A., Garg, S.K., 2012 Recovery factor for EGS, Proc. 37th Workshop on Geothermal Reservoir Engineering, Stanford University.

Hartline, C.S., Walters, M.A., Wright, M.C., 2015, Three-dimensional structural model building, induced seismicity analysis, and reservoir management at The Geysers Geothermal Field, Northern California. GRC Trans. 39, 603-614.

Hauksson, E., Unruh, J., 2007, Regional tectonics of the Coso geothermal area along the intracontinental plate boundary in central eastern California: Three-dimensional V_p and V_p/V_s models, spatial-temporal seismicity patterns, and seismogenic deformation, J. Geophys. Res., 112(B6), B06309, doi:10.1029/2006JB004721.

Hulen, J., Kaspereit, D., Norton, D, Osborn, W., Pulka, F., 2002, Refined Conceptual Modeling and a New Resource Estimate for the Salton Sea Geothermal Field, Imperial Valley, California. GRC Trans 26, 29-36.

Ingebritsen, S.E., Manning, C.E., 2010, Permeability of the continental crust: dynamic variations inferred from seismicity and metamorphism, Geofluids, 10, 193-205.

Jeanne, P., Rutqvist, J., Dobson, P.F., Garcia, J., Walters, M., Hartline, C., and Borgia, A., 2015, Geomechanical simulation of the stress tensor rotation caused by injection of cold water in a deep geothermal reservoir. Journal of Geophysical Research Solid Earth **120**, doi: 10.1002/2015JB012414

Kaspereit, D., Berard, B., Gutierrez, P., Nichols, E., Jiuping, C., 2006, Land and Marine Magnetotelluric Exploration at the Salton Sea Geothermal Field: GRC Trans. 30, pp. 985-989.

Kaspereit, D., Mann, M., Sanyal S., Rickard, B., Osborn, W., Hulen, J., 2016, Updated conceptual model and reserve estimate for the Salton Sea geothermal field, Imperial Valley, California, GRC Trans 40, 57-66.

Kaven, J.O., Hickman, S.H., Davatzes, C., 2011, Micro-seismicity, fault structure and hydraulic compartmentalization within the Coso Geothermal Field, California. Proceedings 36th Workshop on Geotherm. Res. Eng., Stanford University, SGP-TR-191.

Kaven, J.O., Hickman, S.H., Davatzes, N.C., 2013, Micro-seismicity within the Coso geothermal field, California from 1996-2012. Proceedings 38th Workshop on Geotherm. Res. Eng., Stanford University, SGP-TR-198.

Kaven, J.O., Hickman, S.H., Davatzes, N.C., 2014, Micro-seismicity and seismic moment release within the Coso geothermal field, California. Proceedings, 39th Workshop on Geothermal Reservoir Engineering, Stanford University, SGP-TR-202, 10 p.

Knapek, E. Platl, C., 2014, Geothermal Energy in the Munich Metropolitan Area, slide desk accessed on 30-April-2017. http://geodh.eu/wp-content/uploads/2014/02/GeoDH_Offenburg_2014-02_Unterhaching_Knapek.pdf

LBL Induced Seismicity Website: http://esd1.lbl.gov/research/projects/induced_seismicity/

Lees, J.M., 2002, Three-dimensional anatomy of a geothermal field, Coso, southeast-central California, in Glazner, A.F., Walker, J.D., Bartley, J.M., eds., Geologic Evolution of the Mojave Desert and Southwestern Basin and Range: Boulder, Colorado, Geol. Soc. Am. Memoir 195, p. 259–276.

Monastero, F.C., Katzenstein, A.M., Miller, J.S., Unruh, J.R., Adams, M.C., Richards-Dinger, K., 2005, The Coso geothermal field: a nascent metamorphic core complex. Geol. Soc. Am. Bull. 117, 1534-1553.

Neilson, D.L., Garg, S., Koenig, B., Truesdell, A., Walters, M.A., Stark, M., Box, T. Jr., Beall, J.J, 2001, Concept for an Enhanced Geothermal Reservoir at the Geysers. GRC Trans 25, 191-194.

Norton, D.L., Hulen, J.B., 2001, Preliminary numerical analysis of the magma-hydrothermal history of The Geysers geothermal system, California, USA. Geothermics 30, 211-234.

Norton, D.L., Hulen, J.B., 2006, Magma-Hydrothermal Activity in the Salton Sea Geothermal Field, Imperial County, California. GRC Trans. 30, 991-998.

Newmark, R.L., Kasameyer, P.W. Younker, L.W., 1988, Shallow Drilling in the Salton Sea Region: The Thermal Anomaly. J. Geophys. Res. 93 pp. 18.

Oil and Gas Journal, 2009, BP's Tiber one of industry's deepest wells, webpage accessed 30-April-2017. http://www.ogj.com/articles/2009/09/bp-s-tiber-one-of.html

Oklahoma Corporation Commission, 1974, Well record form, stamped Sep 4, 1974. Webpage accessed 30-April-2017. ging.occeweb.com/OG/Well%20Records/00000005/OCC_OG_0G5BFM7_1L8M2C4.pdf

Osadchy, A., 2017, Kola Superdeep, webpage accessed 30-April-2017. http://nauka.relis.ru/06/0205/06205036.htm (in Russian).

Reasenberg, P., Ellsworth W., Walter, A., 1980, Teleseismic evidence for a low-velocity body under the Coso geothermal area. J. Geophys. Res. 85(5), 2471–2483. doi:10.1029/JB085iB05p02471

Rowland, J.V., Simmons, S.F., 2012, Hydrologic, Magmatic, and Tectonic Controls on Hydrothermal Flow, Taupo Volcanic Zone, New Zealand: Implications for the Formation of Epithermal Vein Deposits. Econ. Geol. 107, 427-457.

Rose, P. (Ed.), 2012, Creation of an Enhanced Geothermal System through Hydraulic and Thermal Stimulation. Final Report DE-FC07-01ID14186.

Sabin, A., 16 others, 2015, Geologic Setting of the Proposed West Flank Forge Site, California: Suitability for EGS Research and Development. GRC Trans 39, 345-352.

Sabin, A., 18 others, 2016, Geologic setting of the West Flank, a FORGE site adjacent to the Coso geothermal field, Proceedings, 41st Workshop on Geothermal Res. Eng.

Saishu, H., Okamoto, A., and Tsuchiya, N., 2014, The significance of silica precipitation on the formation of the permeable–impermeable boundary within Earth’s crust, Terra Nova, 26, 253-259.

Sanyal, S.K., Enedy, S.L., 2011, Fifty years of power generation at the Geysers geothermal field, California – the lessons learned. 36th Workshop Geothermal Res. Eng., Stanford University, SGP-TR-191.

Sanyal, S.K., Sarmiento, Z., 2005, Booking geothermal energy reserves, GRC Trans. 29, 467-474.

Schmitt, A.K., Martin, A, Stockli, D.F., Farley, K.A., Lovera, O.M, 2012, (U-Th)/He zircon and archaeological ages for a late prehistoric eruption in the Salton Trough (California, USA). Geology, doi: 10.1130/G33634.1

Scholz, C., 2002, The Mechanics of Earthquakes and Faulting, Cambridge University Press, 152p.

Simon, J.I., Vazquez, J.A., Renne, P.R., Schmitt, A.K., Bacon, C.R., Reid, M.R., 2009, Accessory mineral U-Th-Pb ages and $^{40}Ar/^{39}Ar$ eruption chronology, and their bearing on rhyolitic magma evolution in the Pleistocene Coso volcanic field, California. Contrib. Mineral. Petrol. DOI 10.1007/s00410-009-0390-9.

Smith, R.L., Shaw, H.R., 1975, Igneous-related geothermal systems, In: Assessment of Geothermal Resources of the United States – 1975, D.E. White, D.L. Williams, Eds., US Geol. Surv. Circular 726, 58-83.

Smith, R.L., Shaw, H.R., 1978, Igneous-related geothermal systems, In: Assessment of Geothermal Resources of the United States – 1978, L.J.P. Muffler, Ed., US Geol. Surv. Circular 790, 12-17.

Southern California Earthquake Data Center Website: https://service.scedc.caltech.edu/eq-catalogs/date_mag_loc.php.

Stark, M.A., 1990, Imaging injected water in the Geysers reservoir using microearthquake data. GRC Trans. 14, 1697-1704.

Stark, M., 2003, Seismic evidence for a long-lived enhanced geothermal system (EGS) in the northern Geysers Reservoir. GRC Trans. 27, 727-731.

Stimac, J., Goff, F., Wohletz, K., 1997, Thermal Modeling of the Clear Lake Magmatic System, California: Implications for Conventional and Hot Dry Rock Geothermal Development. Los Alamos National Laboratory Report LA-12778-MS, 38p.

Tester, J.W., Anderson, B.J., Batchelor, A.S., Blackwell, D.D., DiPippo, R.E., Drake, M.J., Garnish, M. Livesay, B. Moore, M.C., Nichols, K., Petty, S., Toksoz, M.N., Veatch, R.W., 2006, The Future of Geothermal Energy: Impact of Enhanced Geothermal Systems (EGS) on the United States in the 21st Century. Cambridge, MA, INL/EXT-06-11746.

Tsuchiya, N., Hirano, N., 2007, Chemical reaction diversity of geofluids revealed by hydrothermal experiments under sub- and supercritical states, Island Arc, 16, 6-15.

Unruh, J.R., Twiss, R.J., Monastero, F.C., 2004, Relation between local strain perturbations and relief on the brittle-ductile transition zone, Coso Range, Eastern California. GRC Trans. 28, 681-685.

USGS, 1979, Assessment of Geothermal Resources of the United States -1978, Circular 790. https://pubs.usgs.gov/circ/1979/0790/report.pdf

Walters, M.A., Combs, J., 1991, Heat Flow in the Geysers-Clear Lake Geothermal area of northern California, U.S.A. GRC Monograph on The Geysers Geothermal Field, Special Report No. 17, p. 43-53.

Walters, M.A., Haizlip, J.R., Sternfeld, J.N., Drenick, A.F., Combs, J., 1992, A vapor-dominated high-temperature reservoir exceeding 600°F at The Geysers California, Proc. 13th Workshop on Geothermal Res. Eng., 73-81.

Walters, M., Beall, J.J., 2002, Influence of Meteoric Water Flushing on Noncondensible Gas and Whole-Rock Isotope Distributions in the Northwest Geysers. GRC Trans. 26, p. 379-383.

Watanabe, N., Numakura, T., Sakaguchi, K., Saishu, H., Okamoto, A., Ingebritsen, S.E., Tsuchiya, N., 2017, Potentially exploitable supercritical geothermal resources in the ductile crust, Nature Geoscience, DOI: 10.1038/NGEO2879.

Williams, C.F., 2007, Updated methods for estimating recovery factors for geothermal resources. Proc. 32nd Workshop on Geothermal Reservoir Engineering, Stanford University, SGP-TR-183, 7 p.

Williams, C.F., 2010, Thermal energy recovery from enhanced geothermal systems – evaluating the potential from deep, high-temperature resources. Proc. 35th Workshop on Geothermal Reservoir Engineering, Stanford University.

Williams, C.F., 2014, Evaluating the volume method in the assessment of identified geothermal resources. GRC Trans. 38, 967-974.

Wilmarth, M., Stimac, J., 2015, Power Density in Geothermal Fields, Proceedings of the World Geothermal Congress 2015, Melbourne, Australia.

Wilson, C.K., Jones, C.H., Gilbert, H.J., 2003, A single-chamber silicic magma system inferred from shear-wave discontinuities of the upper crust and uppermost mantle, Coso geothermal area, California: J. Geophys. Res.108, 226, doi:10.1029/2002JB001798.

Zhang, Q., Lin, G., 2014, Three-dimensional V_p and V_p/V_s models in the Coso geothermal area, California: Seismic characterization of the magmatic system. J. Geophys. Res. 119, 4907–4922.